Journal of Power Sources 212 (2012) 233–246

Contents lists available at SciVerse ScienceDirect

Journal of Power Sources

journal homepage: www.elsevier.com/locate/jpowsour

Optimisation of performance through electrode formulation in conversion materials for lithium ion batteries: Co_3O_4 as a case example

Alexandre Ponrouch, M. Rosa Palacín*

Institut de Ciència de Materials de Barcelona, (ICMAB-CSIC), Campus de la UAB, 08193 Bellaterra, Catalonia, Spain

ARTICLE INFO

Article history:
Received 10 February 2012
Received in revised form
29 March 2012
Accepted 3 April 2012
Available online 13 April 2012

Keywords:
Energy storage
Conversion reactions
Tape casting
Lithium batteries
Formulation
Electrochemical impedance spectroscopy

ABSTRACT

A systematic formulation study has been performed on Co_3O_4 based composite electrodes. The influence of diverse parameters has been studied such as: calendaring pressure applied, composition of the composite electrode, nature of the carbon additives (carbon super P, carbon nanofibers and carbon nanotubes) and the size of the active material particles. The influence of electrochemical parameters (lower cut-off voltage, initial C rate, and rate changes or open circuit potential steps during cycling) was also ascertained. These results are discussed in the perspective of the specific issues associated with materials reacting through conversion reactions (first cycle coulombic inefficiency, voltage hysteresis and capacity fade). Finally, basing on electrochemical impedance spectroscopy measurements and systematic record of the IR drop term of the cells upon cycling, a mechanism to account for the generally observed capacity fade on these materials is proposed.

1. Introduction

Li-ion batteries have attracted significant interest since their commercialization in 1991. Nowadays, compounds reacting through three different reaction mechanisms [1] have been identified as battery electrode materials namely, conventional intercalation of Li ions, alloying with Li [2] and conversion reactions [3]. Conversion reaction is the term applied to define the electrochemical reaction of a binary transition metal compound, M_aX_b (M = transition metal, X = O, S, F, P, N,…) with lithium to yield metallic nanoparticles embedded in a matrix of Li_cX. When compared to intercalation electrodes, alloying and conversion type materials share the same advantages (i.e. higher specific capacity) and drawbacks (i.e. larger hysteresis and lower capacity retention). Alloying type materials have recently become a commercial reality thanks to significant progresses in electrode engineering. Conversion reaction electrodes are much less mature and still far from the market and even if electrode formulation has been proved to have a paramount importance in electrochemical performance for other types of materials [4,5], the formulation of conversion type materials has drawn much less attention. Nonetheless, promising results have already been reported for such systems [6–8].

$$M_aX_b + (b\cdot c)Li^+ + (b\cdot c)e^- = a\,M + b\,Li_cX \quad (1)$$

In addition to the specific issues associated with materials reacting through conversion reaction (i.e. Voltage hysteresis and first cycle coulombic efficiency, cf. Ref. [3]), it has also been pointed out by several groups that conversion material at the nanoscale suffer from very poor capacity retention upon cycling as compared to material at the microscale [9,10,7]. Transition metal oxides have attracted most of the attention since Poizot et al. highlighted their reactivity with Li [11]. Among these studies, cobalt oxides have probably attracted most of the attention due to their high theoretical gravimetric capacity, for instance ca. 890 mAh g^{-1} in the case of Co_3O_4. Capacity fade for cobalt oxide electrodes has been ascribed to three different phenomena, namely i) cobalt dissolution [8], ii) contact loss due to volume change during conversion reaction (about 100%), this phenomenon being enhanced in the case of larger particles [12] and iii) formation of a poorly conductive solid electrolyte interface (SEI) and a gel-like film due to electrolyte decomposition inducing higher cell resistivity and poisoning of the Li metal electrode by diffusion of the decomposition products [13–15]. In order to deal with all those parameters, it is of tremendous

* Corresponding author. Tel.: +34 935801853; fax: +34 935805729.
E-mail address: rosa.palacin@icmab.es (M.R. Palacín).

0378-7753/$ – see front matter © 2012 Elsevier B.V. All rights reserved.
doi:10.1016/j.jpowsour.2012.04.005

importance that the composite electrode is perfectly homogeneous and that the three-point contact interface between the active material (AM), the Carbon additive (Cadd) and the electrolyte is optimized so as to ensure that the differences in the electrochemical behaviour do not come from inhomogeneous current density within the electrode. We have previously demonstrated the influence of the mixing of the slurry on the homogeneity of the tape casted electrode and the strong beneficial impact of a sonication procedure [16]. This methodology has thus been used for all electrodes shown here. In this paper, a systematic study of the formulation of Co_3O_4 casted composite electrodes is presented. The influence of several parameters, such as the pressure, the proportion of the AM, the Cadd and the binder, the nature of the Cadd, the particle size and the cycling rate, are correlated with the capacity retention and the electrochemical behaviour of the composite electrodes.

2. Experimental

Nano-sized Co_3O_4 (Aldrich) was previously annealed at 400 °C under air to achieve its nominal oxygen content (as confirmed by thermo gravimetric analysis experiments). The duration of the treatment was changed so as to achieve different particle sizes. The nanometric size of the pristine commercial material is preserved when the heat treatment is limited to 6 h (cf. Fig. 1a) and particle sizes of ca. 35 ± 5 nm are observed. Longer heat treatment periods lead to a significant increase of the particle size reaching, respectively, 50 ± 10 nm and 100 ± 20 nm after 15 and 96 h (cf. Fig. 1b and c).

In all cases slurries were prepared by mixing AM, polyvinylidene fluoride (PVDF, Arkema) as a binder and Super P carbon (Csp hereafter from Timcal), carbon nanotubes (CNT, Thomas Swan Co. Ltd) purified following the procedure described in Ref. [17] or carbon nanofibers (VGCF, Showadenko) as carbon additive (Cadd hereafter) in *N*-Methylpyrrolidone (NMP, Aldrich). Mixing of the slurries was performed (according to Ref. [16]) by magnetic stirring during 15 h, the vial containing the slurry being placed in an ultrasonic bath for 10 min every 5 h. In all cases, the mixing procedures have been performed under air. Composite electrodes were prepared by tape casting each slurry on a 20 μm thick copper foil (Goodfellow) with a 250 μm Doctor-Blade and further dried at 120 °C under vacuum. Once dried, 0.8 cm^2 disk electrodes were cut, pressed at pressures ranging from 0 up to 10 t cm^{-2} and tested in Swagelok type cells with a disk of Li metal foil (Chemetall) as counter and reference electrode (all potentials in this work are referred to Li^+/Li). Two sheets of Whattman GF/d borosilicate glass fibre were used as a separator, soaked with the electrolyte (ca. 0.5 cm^3 of 1 M $LiPF_6$ in EC:DMC 1:1 (LP30, Merck)). Table 1 lists the experimental conditions for electrodes presented in this work, including the calendaring pressure, the composition and the nature of the AM, the Cadd and the binder. Electrochemical cycling experiments were made in galvanostatic mode with potential limitation (GCPL) using a Bio-Logic VMP3 potentiostat. Reproducibility was checked by assembly of twin cells. A systematic cycling procedure was used in all cases. Successions of 10 cycles at different C rate were applied to check the electrochemical behaviour at these rates and determine whether high rates were detrimental to the electrode performance. First, 10 cycles were performed at C/5 followed by 10 cycles at C, C/5, 2C and finally C/5 (1C being one Li^+ inserted in 1 h).

Electrochemical impedance spectroscopy (EIS) measurements were performed upon cycling using three electrode Swagelok cells configuration with Li as counter and reference electrode and a formulated electrode as working electrode. Perturbation amplitudes of 10 mV were applied with frequencies ranging from 1000 kHz to 10 mHz. Measurements were done at the end of charge after an open circuit potential period of 24 h.

Scanning electron microscopy (SEM) studies were performed using a Quanta 200 ESEM FEG FEI microscope. BET surface area measurements were done using a ASAP 2000 Micromeritics instrument.

3. Results

All electrodes were submitted to the standard cycling procedure described in the experimental section and exhibit the expected behaviour for Co_3O_4 (see Fig. 2b). Indeed, the first reduction exhibits three components: i) a first plateau at ca. 1.25 V vs Li^+/Li (thereafter called α), associated with a lithium insertion process and formation of a Li–Co–O intermediate phase [7], ii) a second plateau at ca. 1.15 V vs Li^+/Li (thereafter called β), which is related to the conversion process itself that lead to the formation of Co nanoparticles embedded in a Li_2O matrix, and iii) an almost linear potential decay below 1.15 V vs Li^+/Li (γ), typically observed in conversion reaction materials which appeared to be mostly related to the electrolyte decomposition [20]. Upon re-oxidation, a large voltage hysteresis is observed together with an important coulombic inefficiency, these features being typical for the conversion reaction materials.

3.1. Influence of pressure

Fig. 2 displays the electrochemical curves obtained with composite electrodes prepared from the same tape (84 wt.% of Co_3O_4, 8 wt.% of PVDF and 8 wt.% of Csp, corresponding to electrodes A to E, respectively, cf. Table 1) and pressed at various pressures (ca. 10, 8, 6 and 3 t). The results obtained for an unpressed electrode are also presented for the sake of comparison (noted 0 t). The plot of the capacity vs the number of cycles is shown in Fig. 2a. Mainly three facts are worth pointing out:

(i) During the first cycle, the composite electrodes behaved very much the same and first discharge capacities as high as ca. 1400 mAh g^{-1} were measured in all cases. This point is further

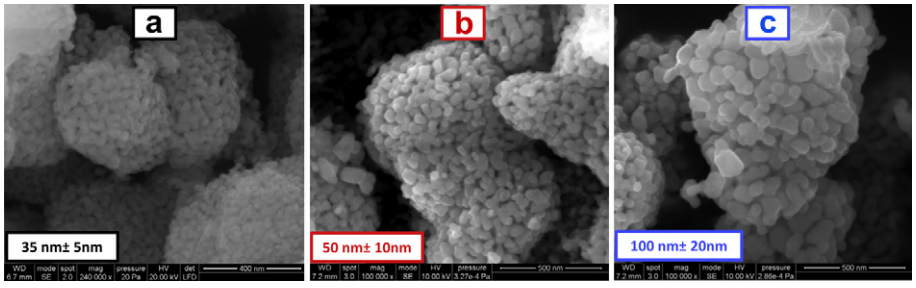

Fig. 1. SEM micrographs of Co_3O_4 heat treated at 400 °C during a) 6 h, b) 15 h and c) 96 h.

Table 1
Calendaring pressure and composition for all electrodes tested in this study including annealing time (directly related to Co_3O_4 particle size, see text).

Electrode	Pressure (t)	Co_3O_4		Cadd		Binder	
		Annealing time (h)	Percentage	Type	Percentage	Type	Percentage
A	0	6	84	Csp	8	PVDF	8
B	3	6	84	Csp	8	PVDF	8
C	6	6	84	Csp	8	PVDF	8
D	8	6	84	Csp	8	PVDF	8
E	10	6	84	Csp	8	PVDF	8
F	8	6	75	Csp	12.5	PVDF	12.5
G	8	6	65	Csp	17.5	PVDF	17.5
H	8	6	75	Csp	17	PVDF	8
I	8	6	65	Csp	27	PVDF	8
J	8	6	65	Csp	31	PVDF	4
K	8	6	65	Csp/VGCF	13.5/13.5	PVDF	8
L	8	6	65	Csp/CNT	13.5/13.5	PVDF	8
M	8	6	84	Csp/VGCF	4/4	PVDF	8
N	8	15	65	Csp	27	PVDF	8
O	8	96	65	Csp	27	PVDF	8

confirmed by the good overlapping of the first cycle for all electrodes in the voltage vs capacity profiles (see Fig. 2b), emphasizing the accuracy of the active material mass measurement in our tape technology as well as the excellent reproducibility of the measurement from one electrode to another coming from the same tape. It is also worth mentioning that in all cases the capacity at the end of the conversion plateau (β) during the first discharge is ranging from 850 up to 890 mAh g^{-1}, thus representing more than 95% of the theoretical specific capacity of Co_3O_4 (ca. 890 mAh g^{-1}).

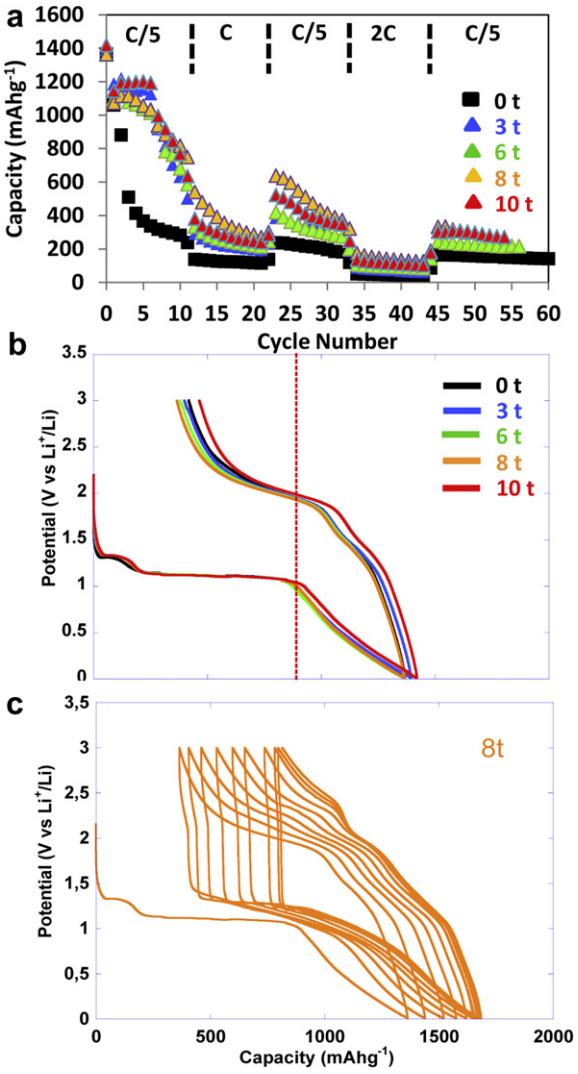

Fig. 2. a) Discharge capacity vs cycle number for electrodes A to E tested in half cells. b) First cycle voltage vs capacity profiles for the same tests and c) first ten cycles for electrode D pressed at 8 t cm^{-2}.

(ii) There is an important difference between pressed (ca. 3, 6, 8 and 10 t) and unpressed electrodes in terms of capacity retention upon cycling. Indeed, as it can be observed in Fig. 2a, the unpressed electrode experienced an important capacity decay during the first cycles, whereas the pressed electrodes maintained a good capacity (about ca. 1100 mAh g^{-1}) for at least seven cycles before experiencing a slow capacity decay. Interestingly, this capacity fade has been observed associated with the apparition of an additional oxidation pseudo plateau at about 2.75 V vs Li^+/Li (cf. Fig. 2c).

(iii) Composite electrodes pressed at 8 t appeared to present the best capacity retention, thus this pressure was applied to all electrodes presented later on in this work. Indeed, capacities measured at C/5 after a sequence of 10 cycles at C are, ca. 238, 389, 420, 639 and 523 mAh g^{-1}, respectively, for composite electrodes being pressed at ca. 0, 3, 6, 8 and 10 t. The same trend is observed throughout the cycling procedure and demonstrates a significant improvement of the capacity retention by pressing the electrode at 8 t. A slight decrease of the capacity retention was observed when the electrode was pressed at 10 t, most probably due to electrolyte percolation limitation within highly dense electrodes [18].

3.2. Influence of the slurry composition

Three sets of experiments were designed in order to take into account the specific influence of the AM, the Cadd and the binder content within the slurry. The results are reported in Fig. 3. First, the proportion of AM was varied between 84 and 65 wt.%, the ratio between Cadd and binder (PVDF) being fixed to 50:50 (electrodes D, F and G). Fig. 3a shows the plot of the capacity vs the number of cycles for these electrodes using the same standard cycling procedure described in the experimental section. Interestingly, the first cycle is very similar in all cases and first discharge capacities as high as 1300 mAh g^{-1} are obtained, suggesting a contribution of the whole active material mass. However, from the voltage vs capacity profiles of the first cycle (data not shown) we can estimate than the capacity at the end of the conversion plateau (β) vary from 865 to 795 mAh g^{-1} (ca. 97–89% of the theoretical specific capacity of Co_3O_4) when the AM content was varied, respectively, from 84 to

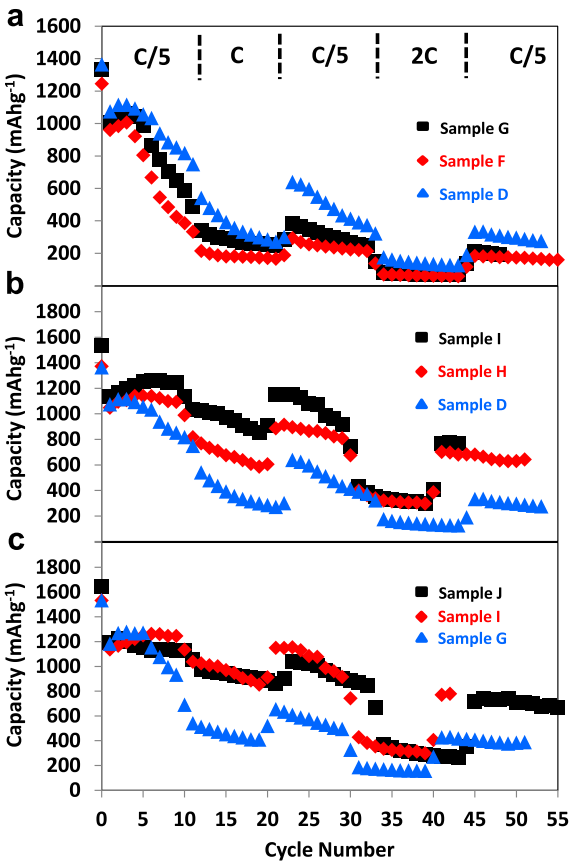

Fig. 3. a) Discharge capacity vs cycle number for a) electrodes G, F and D, b) electrodes I, H and D and c) electrodes I, J and G, tested in half cells.

65% wt.%. Furthermore, while the first three cycles present similar reversible capacities around 1000 mAh g^{-1}, an important capacity fade is observed after four cycles and the best capacity retention was obtained for electrode D (84 wt.% of CO46, 8 wt.% of PVDF and 8 wt.% of Csp). These results are surprising as the electrode with the highest AM content presents the higher AM utilisation together with the best capacity retention. Still, it should be kept in mind that the ratio Cadd/binder being fixed, the electrode with the highest AM content exhibits lowest binder content. It seems straightforward to conclude that a large amount of binder (PVDF here) lowers the AM utilisation and enhances capacity fading, most probably by electrical isolation of the AM particles due to the insulating nature of PVDF.

In order to better understand the influence of the Cadd and the binder contents, two other sets of experiments were performed: i) The AM content was varied between 84 and 65 wt.%, but this time maintaining a fixed PVDF content of 8 wt.% (electrodes D, H and I, cf. Fig. 3b) and ii) The AM content was fixed at ca. 65 wt.%, while the PVDF content was varied from 4 up to 17.5 wt.% (electrodes J, I and G, cf. Fig. 3c).

In the first case, as we can see from the plot of the capacity vs the number of cycles (cf. Fig. 3b) the first discharge capacity value appeared to be slightly larger for electrode I (65 wt.% of AM and 8 wt.% of PVDF) compared to higher AM content with the same binder content. This can be attributed either to a slightly better electrical contact and thus utilisation of the AM (due to the higher amount of Cadd) and/or to an increase of the capacity contribution of the irreversible solid electrolyte interface (SEI) formation on Csp. The latter hypothesis is in agreement with the fact that this difference disappeared after the first discharge (cf. Fig. 3b) and that in all cases the capacity at the end of the first discharge conversion plateau (β) represent more than 95% of the theoretical specific capacity of Co_3O_4 suggesting full AM utilisation in all the electrodes. More importantly, the capacity retention appeared to be strongly influenced by the AM content and even if electrodes present similar reversible capacities during the first five cycles (around ca. 1100 mAh g^{-1}) the capacity retention appeared to drastically improve when varying the AM content from 84 to 65 wt.%. It is worth recalling that this variation of AM content is concomitant with the variation of Cadd and that the best capacity retentions were achieved with the lowest amount of AM and the highest content of Cadd. These results suggest that a key issue for the long term cycling of Co_3O_4 is the electrical contact with the AM. In order to optimize this contact the AM content of the tapes were fixed at 65 wt.% for the following experiments of this study.

The last set of experiments was performed in order to determine an optimal value for the binder content. The AM content was fixed at 65 wt.% and the binder content was varied from 4 to 17.5 wt.% (electrodes J, I and G, cf. Fig. 3c). As previously mentioned the value of the first discharge is slightly different and varied from 1400 to 1600 mAh g^{-1} when the Cadd content is varied from 17.5 to 31 wt.% (respectively for electrodes G, I and J, cf. Fig. 3c). Once again this difference disappears during the next cycles and reversible capacities around 1200 mAh g^{-1} are recorded for the first few cycles. However, while electrodes J and I present very good and similar capacity retentions with reversible capacities around 800 mAh g^{-1} at C/5 after more than fifty cycles, electrode G experiences an important capacity fade after 6 cycles (cf. Fig. 3c). Keeping in mind that electrode G contains 17.5 wt.% of insulating PVDF binder it seems straightforward to conclude that once again the electrical contact with the AM is the key factor for good capacity retention, and using a high amount of insulating binder strongly impedes the capacity retention of the electrode. Furthermore, the capacity at the end of the first discharge conversion plateau (β) was more than 95% of the theoretical specific capacity of Co_3O_4 for electrodes I and J, and only 88% for electrode G, once again suggesting that a high PVDF content induces an electrical isolation of the AM particles, making them electrochemically inactive. A PVDF content of 4 wt.% (electrode J) induced a poor mechanical stability of the composite electrodes and, therefore, a binder content of 8 wt.% was fixed for all following experiments as a good compromise between the mechanical stability and the electrochemical performance of the electrodes.

3.3. Influence of the type of C (Csp, MWCNT, VGCF)

According to the previous results, the AM and the binder contents were fixed to, respectively, 65 and 8 wt.%. In order to evaluate the influence of the nature of the Cadd, three compositions of Cadd were studied and tested according to the same standard cycling procedure described in the experimental section. In all cases, the total content of Cadd was fixed to ca. 27 wt.%. For electrode I the Cadd was only Csp, electrode K was constituted of a mixture of 13.5 wt.% of Csp and 13.5 wt.% of VGCF, and for electrode L a Cadd mixture of 13.5 wt.% of Csp and 13.5 wt.% of CNT was used. Fig. 4a displays the plot of the capacity vs the number of cycles for these three electrodes. The first discharge capacity strongly depends on the nature of the Cadd with values around 1530, 1540 and 1870 mAh g^{-1} respectively for Csp, Csp + VGCF and Csp + CNT. As previously noticed, this trend seems to follow the surface area of the C exposed. Indeed, the specific BET surface areas of Csp, VGCF and CNT are, respectively, 54, 18 and 304 $m^2 g^{-1}$ and should be proportional to the irreversible formation of an SEI layer on the carbon during the first discharge. This is in agreement with the values of the first cycle coulombic efficiency recoded ca. 66, 67

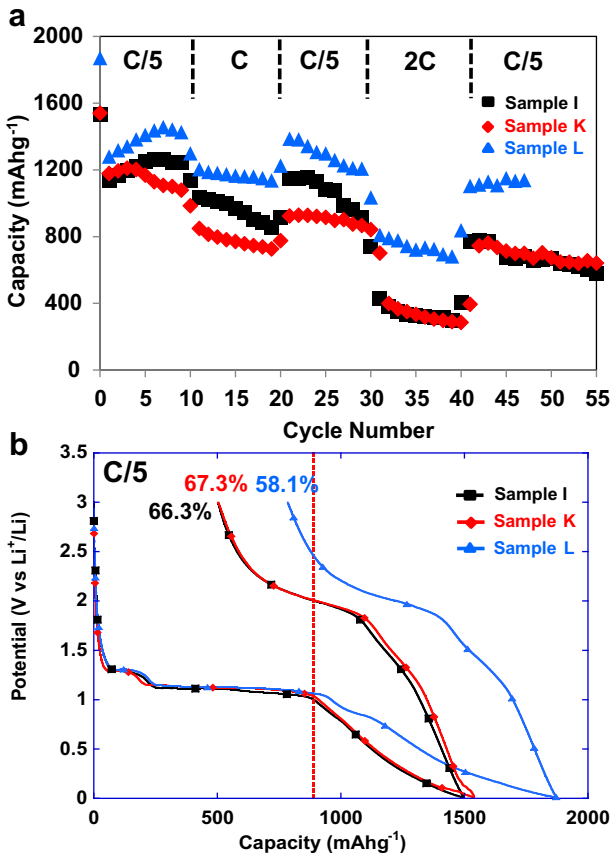

Fig. 4. a) Discharge capacity vs cycle number for electrodes I, K and L. b) First cycle voltage vs capacity profiles for the same tests (recorded at C/5).

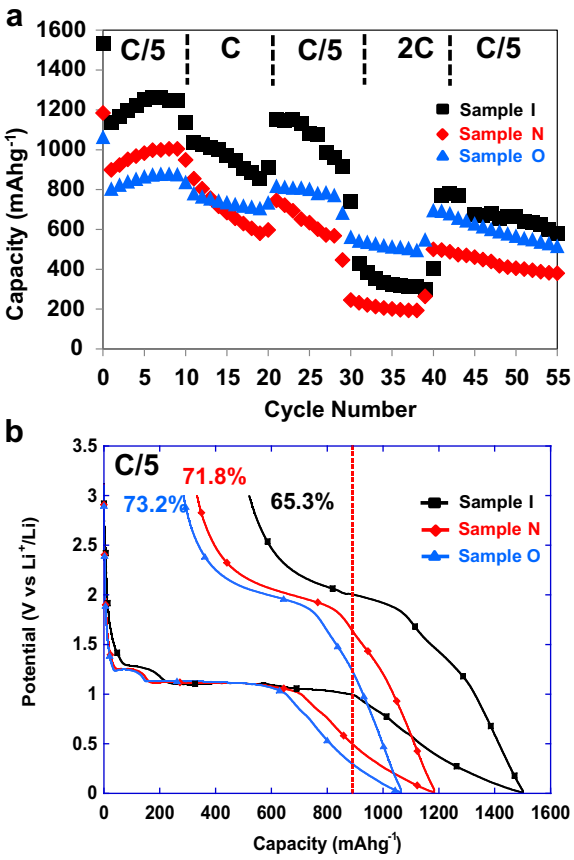

Fig. 5. a) Discharge capacity vs cycle number for electrodes I, N and O. b) First cycle voltage vs capacity profiles for the same tests (recorded at C/5).

and 58%, respectively, for Csp, Csp + VGCF and Csp + CNT (cf. Fig. 4b). Unique features are visible in the voltage vs capacity profiles (cf. Fig. 4b) for electrodes containing VGCF and CNT. A pseudo plateau is observed at about 0.8 V vs Li^+/Li for electrode L probably due to electrolyte decomposition and formation of an SEI layer on CNT [19]. At lower potentials electrodes K and L exhibit significantly larger reversible capacity which is possibly related to the insertion of Li^+ between the graphene layers of VGCF and CNT. However, no significant change on the capacity retention was achieved by substituting Csp with VGCF as Cadd for well formulated electrodes based on Co_3O_4. This is in agreement with Ref. [4] for Si based electrodes, suggesting that the electronic wiring throughout the electrode with only Csp as the Cadd is satisfactory.

3.4. Influence of the particle size

The control of particle size is of primary importance since it has been reported [7,9,10] that particles smaller than 50 nm demonstrate poor capacity retention while mesoporous or micron sized particles exhibit much better performance. It was then suggested that enhanced electrolyte decomposition for nanoparticles was the main cause for this poor behaviour.

In order to better understand this issue we performed the same standard cycling procedure as in the previous sections to electrodes prepared with particle sizes ranging from 35 to 100 nm (Fig. 1 and electrodes I, N and O, cf. Table 1). The results are displayed in Fig. 5, where two main features can be pointed out:

i) The specific capacities appear to be inversely proportional to the particle size. For instance, about ca. 1500, 1200 and 1050 mAh g^{-1} were measured as first discharge capacities, respectively, for electrodes I (35 ± 5 nm), N (50 ± 10 nm) and O (100 ± 20 nm) (cf. Fig. 5). The same trend is observed during the first ten cycles at C/5 (reversible capacities of ca. 1250, 1000 and 850 mAh g^{-1} are recorded, respectively, for electrodes I, N and O at the tenth cycle). Keeping in mind that the theoretical capacity for Co_3O_4 is 890 mAh g^{-1}, this suggests that the well-known extra capacity for materials reacting through conversion reaction [3] is decreased/suppressed in the case of particles larger than 50 nm and that full AM utilisation is achieved in all cases.

ii) After ten cycles and the C rate being switched to 1C, a significant difference was observed between electrode O (particle size of about ca. 100 nm) with good capacity retention and the others (I and N) exhibiting important capacity fade.

It is also worth mentioning that coulombic efficiencies were found to be dependent on the particle size. As we can see from Fig. 5b, the first cycle coulombic efficiency increased from 65 up to 73% when the particle size increased from 35 ± 5 nm up to 100 ± 20 nm. The same trend is observed upon cycling and coulombic efficiencies of ca. 99% (at all C rates) are recorded in the case of 100 nm particles, whereas only 92% are obtained for 35 ± 5 nm particles. Interestingly, for 35 ± 5 nm particles (electrode I) coulombic efficiency increased when the C rate was increased and reached, respectively, 95 and 97% at 1C and 2C. The good capacity retention observed for this electrode is quite surprising. Indeed, it was reported by several groups that such small particles experience very strong capacity fading after less than ten cycles [7,9,10].

These results suggest a strong influence of the electrolyte decomposition on the capacity retention upon cycling, as pointed out by Grugeon et al. [10], decreasing the particle size enhances the decomposition kinetics and lowers the capacity retention. The fact that the coulombic efficiency increases when the C rate is increased demonstrate that the electrolyte decomposition and the conversion reaction are two processes with different kinetics, the latter being faster, in agreement with Ref. [20]. Finally, the fact that capacity at 2C are larger for 100 nm particles than for 35 nm particles suggest that electrolyte decomposition products somehow hindered the kinetics of the conversion reaction and/or limit the electrochemical activity of the AM.

3.5. Influence of the electrochemical testing protocol

In Section 3.4 we have pointed out that a possible reason for the poor capacity retention of Co_3O_4 nanoparticles with particle size below 50 nm could be rooted in the by-products formed during electrolyte decomposition. This phenomenon can be further investigated by playing with two parameters: i) the lower cut-off voltage, the decomposition of the electrolyte being enhanced at low potentials and ii) the C rate, the kinetics of the electrolyte decomposition being slower than for the conversion reaction [20].

Fig. 6a presents the plot of the capacity vs cycle number for electrode D cycled between *x* and 3 V vs Li^+/Li, *x* being 0.01, 0.2 or 0.5 V vs Li^+/Li. As we can see, and as it was already reported by Grugeon et al. for CoO particles [13], the lower cut-off potential has a very strong influence on the capacity retention. Indeed, the capacity retention was found to be strongly enhanced when lowering the cut-off voltage, the best value being obtained for 0.01 V vs Li^+/Li, in agreement with [13], who ascribed this results to the necessity of the polymeric gel-like film to be present in order to achieve a good cyclability of the electrode.

The influence of the initial C rate has also been studied and several identical electrodes (electrode I, cf. Table 1) have been submitted to C rates ranging from C/5 up to 10C. The plot of the capacity vs the number of cycles is shown in Fig. 7a and, as we can see, satisfactory capacity values are obtained even at high C rates with such formulated electrodes. Indeed, first discharge capacities ranging from 1030 up to 1490 mAh g^{-1} were recorded for C rates from 10C to C/5, respectively. The capacity recorded at the end of the conversion plateau (β) during the first discharge is significantly reduced by increasing the C rate (cf. Fig. 7b), suggesting that the conversion reaction is diffusion limited and that the bulk of the Co_3O_4 particles is not completely accessible for the Li^+ ions at high C rate. Indeed, while almost 100% of the Co_3O_4 theoretical capacity (ca. 890 mAh g^{-1}) is reached at C/5 during the first discharge conversion plateau only 680 mAh g^{-1} is reached at 10C (i.e. 76% of the theoretical capacity). A simple calculation, assuming that diffusion of Li^+ inside the Co_3O_4 particle is the only limiting process and considering spherical Co_3O_4 particles of 35 nm suggests that the conversion reaction only occurs at a 6.6 nm depth inside the Co_3O_4 particles thus resulting in a 21.8 nm diameter inactive Co_3O_4 particles at the end of the first discharge. Similar calculations at 2C and C/5 where, respectively, 850 and 890 mAh g^{-1} are recorded at the end of the first discharge indicate a depth of electrochemical activity of about 11.3 and 17.5 nm, respectively.

High reversible capacities were also obtained during the following cycles: ca. 700 mAh g^{-1} were measured at a C rate of 10C demonstrating that a conversion material can perform nicely even at such a high C rate. This observation is in agreement with the results from Taberna et al. [21] who managed to obtain 80% of the

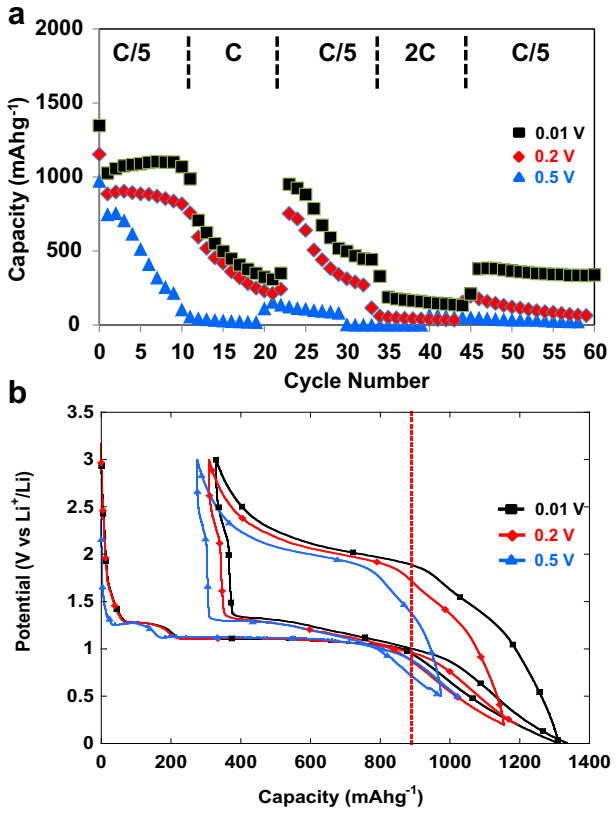

Fig. 6. a) Discharge capacity vs cycle number for electrodes D cycled with a lower cut-off voltage of 0.01, 0.2 or 0.5 V vs Li^+/Li. b) First cycle voltage vs capacity profiles for the same tests (recorded at C/5).

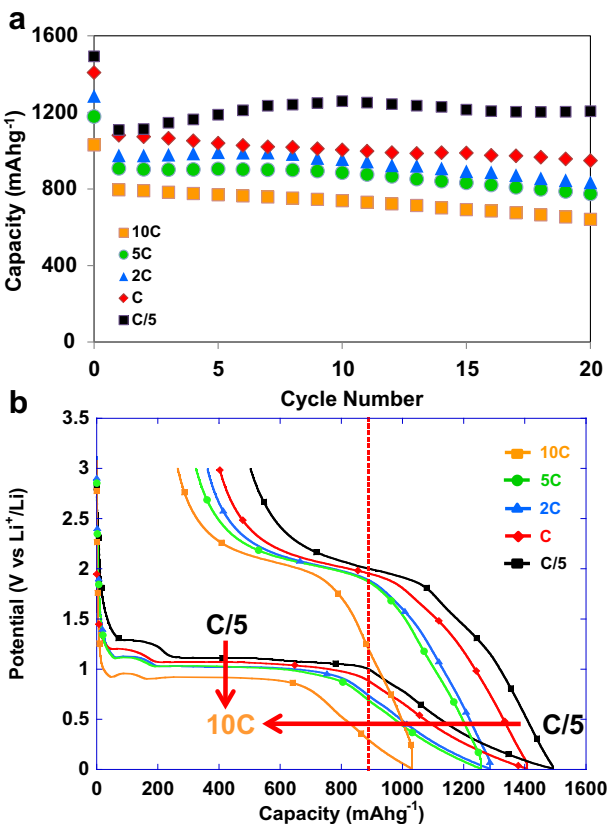

Fig. 7. a) Discharge capacity vs cycle number for electrodes I cycled at a C rate of C/5, C, 2C, 5C or 10C. b) First cycle voltage vs capacity profiles for the same tests.

total capacity at a 8C rate with Fe_3O_4 as AM electrodeposited on an array of Cu nanowires. However, to the best of our knowledge, this is the first time that such high reversible capacities are reported for conversion based composite electrodes at high C rates.

3.6. Long term cycling experiments

Long term cycling (Fig. 8a and b) was performed with identical electrodes cut from the tapes labelled as electrodes I and O (65% of AM, 27% of Csp and 8%of PVDF, the AM being Co_3O_4 particles of 35 ± 5 nm and 100 ± 20 nm, respectively, cf. Table 1) and cycled between 0.01 and 3 V vs Li^+/Li, at C/5, C and 2C during 100 cycles. The C rate was then changed to C/5 in order to evaluate the impact of the C rate change on the cyclability. As we can see from Fig. 8a the first discharge capacity is inversely proportional to C rate and larger values were obtained at C/5 (ca. 1493 mAh g^{-1}) as compared to those recorded at C (ca. 1360 mAh g^{-1}) and 2C (ca. 1220 mAh g^{-1}). However, after the first discharge, similar reversible capacities are obtained at C/5, C and 2C during a few cycles and then the electrodes experience significant capacity fade. Interestingly, this capacity fade appears to be strongly dependent on the C rate applied and mainly two general observations can be pointed out: i) The start of the capacity fade is depending on the C rate and is delayed for higher C rates, for instance capacity fade is observed after 10, 20 and 35 cycles, respectively at C/5, C and 2C; ii) Although delayed, the capacity fade is more important at high C rates. Indeed, from cycle number 35 to cycle number 100, about 60% of the capacity is lost at 2C while only 35 and 0% of the reversible capacity is lost at C and C/5 from the beginning of the capacity fade to cycle number 100.

In the case of electrode O (100 ± 20 nm; see Fig. 8b) the discrepancy in the capacity values observed during the first discharge between C/5, C and 2C is maintained and even enhanced upon cycling resulting in much higher reversible capacities at C/5 compared to C and 2C. Furthermore, the main differences observed between electrodes I (35 ± 5 nm particles) and O (100 ± 20 nm) are: i) the significantly larger capacities recorded for electrode I, and ii) the higher increase of the capacity during the first few cycles as well as the bigger capacity fade observed in the case of electrode I compared to electrode O (cf. Fig. 8a and b). However, it is worth mentioning that switching the C rate at ca. C/5 after 100 cycles at C and 2C, reveals that the electrodes made of 35 nm particles can retrieve full capacities. This suggests that the capacity fade originates from either kinetic or diffusion limitations that can be overcome by decreasing the C rate.

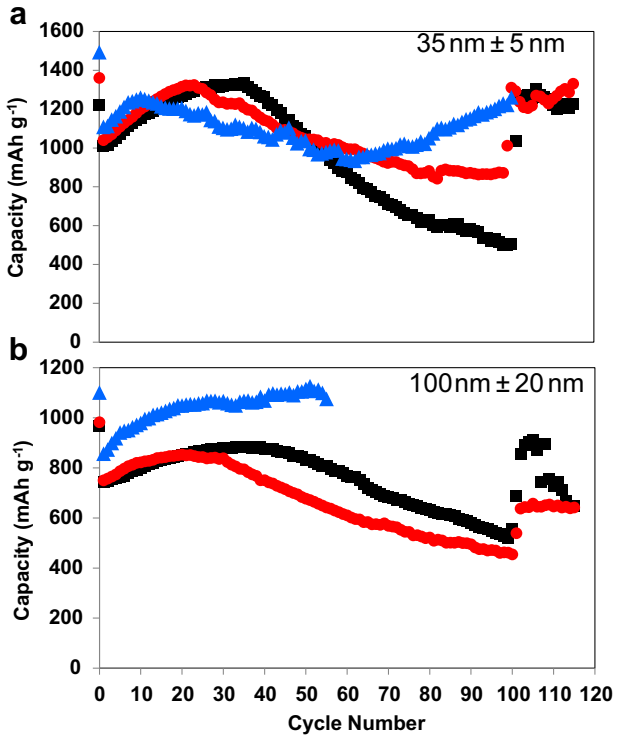

Fig. 8. Discharge capacity vs cycle number recorded at C/5 (black squares), C (red circles) and 2C (blue triangles) for a) electrode I and b) electrode O. In all cases C rate was changed to C/5 after 100 cycles. (For interpretation of the references to colour in this figure legend, the reader is referred to the web version of this article.)

Calculations of the depth of the conversion reaction inside the Co_3O_4 particles give coherent results. Indeed, 100% of the Co_3O_4 theoretical capacity (ca. 890 mAh g^{-1}) is reached at C/5 during the first discharge conversion plateau for electrode I, while only 700 mAh g^{-1} is reached at the same C rate for electrode O (i.e. 78% of the theoretical capacity). The depth of penetration of the conversion reaction inside the Co_3O_4 particles at C/5 is similar (ca. 17 nm) for electrodes O and I. At a 2C rate, values of 15.6 and 11.3 nm are obtained for electrodes O and I respectively. These results are in agreement with the fact that high C rates should induce lower penetration of Li^+ inside the AM particles and that the diffusion coefficient of Li^+ should be equal within a given active material no matter its particle size. To the best of our knowledge, the capacity at the end of the conversion plateau β represents an excellent signature of the AM electrochemical accessibility, as it is always reported in the literature, to be less than or equal to the theoretical capacity of Co_3O_4 (see for instance Refs. [3,6,8,10,11,13,14,16,21]) with the exception of Ref. [22] which report puzzling results with a conversion plateau as large as 2000 mAh g^{-1}.

3.7. Impact of formulation on the specific problems in conversion materials (coulombic efficiency, voltage hysteresis and capacity fade)

In light of the previously described results, we will now discuss in more detail the specific issues associated with materials reacting through conversion reaction, i.e.: i) the coulombic efficiency of the first cycle (difference of capacity recorded between the first discharge and charge), and ii) the large voltage hysteresis between charge and discharge. These will be discussed together with the observed capacity retention in order to better understand the possible mechanisms leading to capacity fading. In this section we further investigate the results presented in Figs. 2 and 3, and 5–8 as they allow direct comparison between electrodes displaying good capacity retention with those presenting poor cyclability depending on both the electrode fabrication/formulation (calendaring pressure, composition and particle size) and electrochemical parameters (low cut-off voltage and C rate).

3.7.1. Coulombic efficiency

Fig. 9 displays plots of the first cycle coulombic efficiencies depending on, respectively, the pressure applied to the electrode (cf. Fig. 9a), the composition of the electrode (cf. Fig. 9b), the Co_3O_4 particle size (cf. Fig. 9c), the low cut-off voltage (cf. Fig. 9d) and the C rate (cf. Fig. 9e). Four important observations can be stressed out from these results:

i) The coulombic efficiency is increased by increasing the pressure and reaches a maximum value of ca. 73.4% for an electrode pressed at 8 t (cf. Fig. 9a). Further increase of the pressure lowers the coulombic efficiency thus probing the effect of calendaring pressure on the electrode porosity.

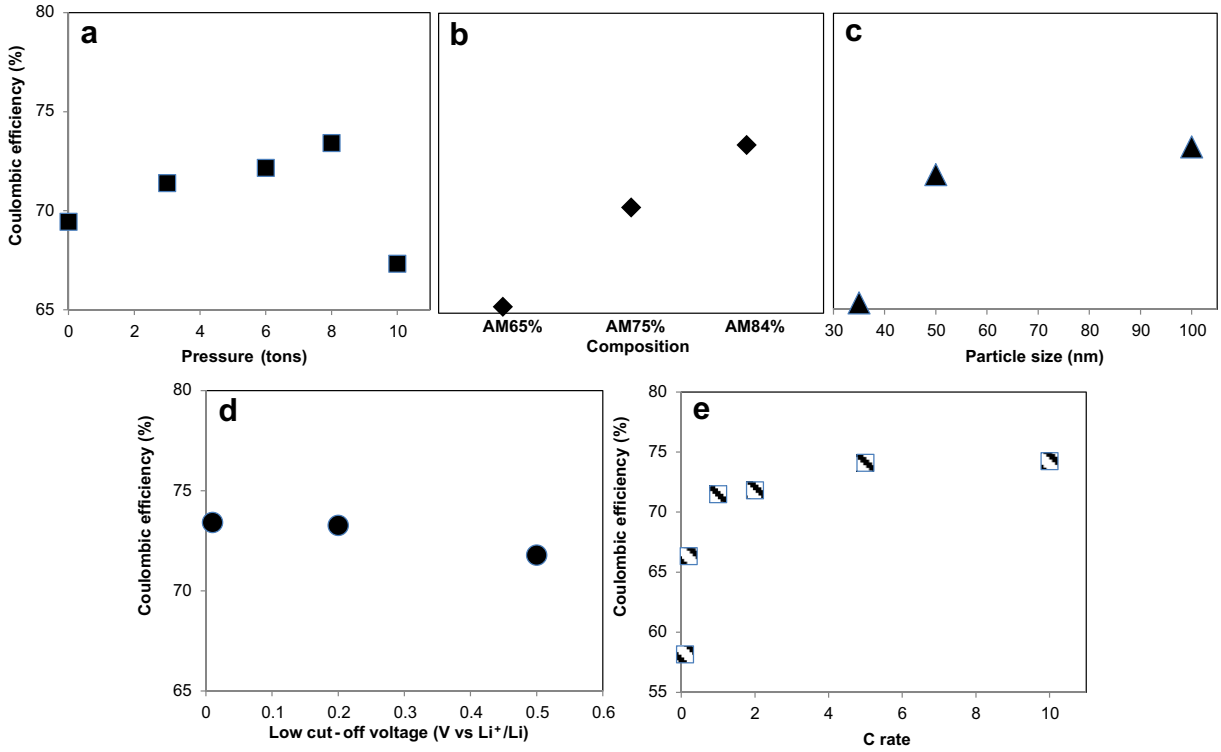

Fig. 9. First cycle coulombic efficiency for the tests presented in a) Fig. 1b, b) Fig. 3b, c) Fig. 7b, d) Fig. 8b and e) Fig. 9b.

ii) As expected, an augmentation of the Cadd content in the electrode results in a coulombic efficiency decrease. This can be clearly seen from Fig. 9b, showing that the coulombic efficiency is ranging from about ca. 65 to 73% when the AM content is varying from 65 to 84%. The binder content was fixed to 8% in all cases, the Cadd content was thus varied from 27 to 8%. This result is consistent with the irreversible formation of the well-known SEI layer on the carbon [23], and suggests that the Cadd content have a stronger impact on the first cycle coulombic efficiency than the Co_3O_4 content.

iii) The particle size appears to significantly affect the coulombic efficiency, the latter being lower for "small" particles (cf. Fig. 9c). This phenomenon does not seem to be linear, the coulombic efficiency being much lower for particle smaller than 50 nm. This result suggests a strong influence of the current density imposed on the AM particles. This is further confirmed by the evolution of the coulombic efficiency with respect to the C rate (i.e. applied current). Indeed, the coulombic efficiency is strongly enhanced by increasing the C rate and ranges from about 58 up to 75% when the C rate is varied from C/10 up to 10C (cf. Fig. 9e). Therefore, it can be concluded that the value of the coulombic efficiency is not only related to the SEI formation on the carbon but also to the electrolyte decomposition on Co_3O_4, the latter being enhanced in the case of particles smaller than 50 nm and for low C rates.

iv) It is also worth mentioning that the coulombic efficiency of the first cycle is not significantly modified when varying the lower cut-off voltage from 0.01 to 0.5 V vs Li^+/Li. This observation is quite surprising. Indeed, the reactions occurring at potentials lower than 1 V vs Li^+/Li are ascribed both to the decomposition of the electrolyte, suggested to be somehow reversible [24] and to the SEI formation on the carbon, which is an irreversible process [25]. Therefore, one would expect a higher cut-off voltage to be beneficial in terms of coulombic efficiency. This is obviously not the case, suggesting an important contribution to the coulombic inefficiency being rooted in the conversion reaction itself, or at least in reactions possibly occurring at higher potential than 0.5 V vs Li^+/Li. This is in agreement with the oxidation of the Co nanoparticles being limited to CoO and not Co_3O_4 as observed in Ref. [26]. Indeed, the maximum columbic efficiency recorded in our experiments was about 75% which corresponds to the re-oxidation of the Co nanoparticles into CoO (theoretical capacity of ca. 715 mAh g^{-1}, i.e. 80% of the Co_3O_4 theoretical capacity) not into Co_3O_4 (theoretical capacity of ca. 890 mAh g^{-1}).

The Υ component (low potential extra capacity related to the electrolyte decomposition and the SEI formation) in the first discharge has been evaluated with respect to these parameters (C rate, Cadd content and particle size; cf. Fig. 10). As expected, the participation of the first discharge capacity to the electrolyte decomposition and the SEI formation is increasing from 33.5 to 40.4%, the C content being varied from 8 to 27 wt.% (cf. Fig. 10b) and from 36.2 to 40.4% with the particle size ranging from 100 to 35 nm (cf. Fig. 10c). It is straightforward to conclude that large Cadd content favours the SEI formation and that Co_3O_4 particle size lower than 50 nm enhance the electrolyte decomposition, both phenomena (SEI formation and electrolyte decomposition) lowering the coulombic efficiency. Interestingly, the Υ component in the first discharge is strongly decreased by increasing the C rate (cf. Fig. 10a) indicating that the conversion reaction kinetics is larger than the one of the process occurring at low potentials. As mentioned elsewhere [20], this is in agreement with the extra capacity at low potential being rooted in slow kinetics processes dealing with electrolyte decomposition (involving catalytic steps), interfacial storage [27], if any, being negligible.

Therefore, from the discussion above, it can be concluded that two major factors limit the coulombic efficiency. The first one is

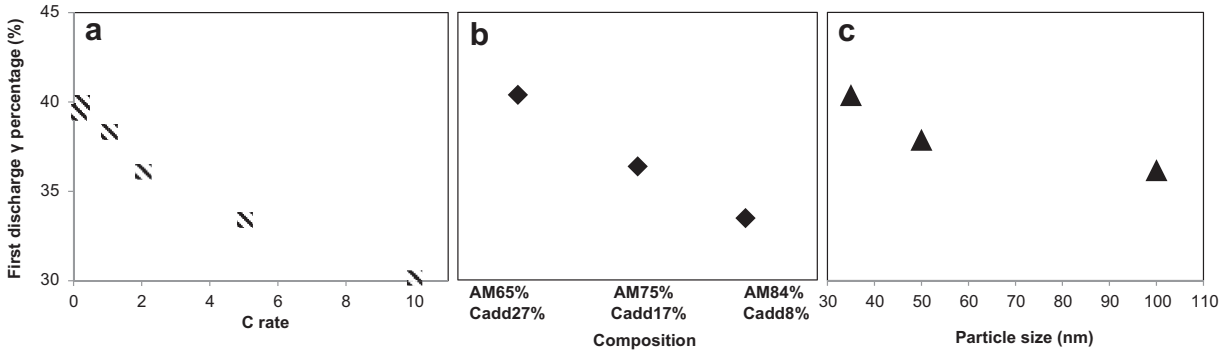

Fig. 10. λ Extra capacity contribution to the first discharge for the tests presented in a) Fig. 9b, b) Fig. 3b and c) Fig. 7b.

intrinsic to the material itself and limits the coulombic efficiency of the electrodes using Co_3O_4 as the AM to 80% because of the partial re-oxidation of the Co nanoparticles (formed at the end of the conversion reaction) into CoO and not into Co_3O_4. The second factor deals with the SEI formation on Cadd and electrolyte decomposition. However, taking this in consideration, excellent coulombic efficiencies, almost reaching the maximal value, were obtained in this study for: i) high C rates (cf. Fig. 9e), ii) small carbon contents (cf. Fig. 9b) and large particle sizes (cf. Fig. 9c).

3.7.2. Voltage hysteresis and capacity fade

The first cycle voltage hysteresis of all the electrodes cycled in this study was evaluated by measuring the difference between the potential at the half first charge capacity and the potential at the middle of the conversion plateau during the first discharge. In all cases a voltage hysteresis of about 0.83 ± 0.03 V was recorded at a C/5 rate. As expected, larger voltage hysteresis were obtained for higher C rates, for instance 1.09 V at 10C. However, even at 10C the IR drop term (measured by the shift of the conversion plateau at lower potential or between the end of the first discharge and the beginning of the first charge)is negligible (less than 0.15 V) compared to the large voltage hysteresis observed between discharge and charge, further demonstrating that this voltage hysteresis is not rooted in the electrode resistivity [21] but most probably originates from thermodynamic issues intrinsic to the conversion reaction [28] and not in technological issues derived from poor electrode formulation.

Some tendencies in the voltage vs capacity profiles are worth pointing out here as they could be correlated with the capacity retention of the electrodes. In order to better illustrate this point and to facilitate the comparison between the voltage vs capacity profiles of different electrodes and their evolution upon cycling, normalized voltage vs capacity profiles, were plotted and are shown in Fig. 11. Normalized voltage vs capacity profiles for electrode I (35 ± 5 nm particles) cycled a hundred times at C/5 and 2C are shown, respectively, in Fig. 11a and b. Similar plots were made for electrode O (100 ± 20 nm particles) at C/5 (cf. Fig. 11c) and 2C (cf. Fig. 11d) for comparison. As we can see in Fig. 11a an oxidation pseudo plateau (thereafter called P_{ox}) appeared upon cycling at about ca. 2.75 V vs Li^+/Li. This phenomenon is concomitant with the shift to lower potential values of the reduction pseudo plateau (thereafter called P_{red}) initially observed at about 2.25 V vs Li^+/Li. After about twenty cycles the reduction pseudo plateau has disappeared and P_{ox} continues to shift upon higher potential values, thus becoming progressively less visible as it reaches the upper cut-off voltage. This observation suggests that the whole capacity recorded comes from at least two different electrochemical processes, one of them presenting an increased overpotential upon cycling, which results in the larger irreversibility of the redox reaction. Interestingly, this increased overpotential upon cycling appears to be much lower at large current density as it can be seen from Fig. 11b–d where no significant shifts of P_{ox} and P_{red} are observed, respectively, for electrode I (35 ± 5 nm particles) cycled at 2C and electrode O (100 ± 20 nm particles) cycled at C/5 and 2C. At this point it is worth reminding that significant capacity fade was observed in the case of electrode I cycled at C/5 after only twelve cycles (cf. Fig. 8a), while much better capacity retention was recorded in the case of electrode I cycled at 2C and electrode O cycled at C/5 or 2C (cf. Fig. 8a and b), thus suggesting that the disappearance of P_{ox} and P_{red} is detrimental to the capacity retention. Similar observations were made in the case of pressed or unpressed electrodes (electrodes A to E), as well as in the study of the influence of the lower cut-off voltage, where the capacity fade was accompanied by the disappearance of P_{ox} and P_{red} (data not shown). This is in agreement with the results from Ref. [7]. The fact that the appearance and disappearance of P_{ox} and P_{red} is faster for high lower cut-off voltage (ca. 0.5 V vs Li^+/Li) compared to lower values tested (ca. 0.2 and 0.01 V vs Li^+/Li), suggests that the phenomenon underlying the appearance/disappearance of P_{ox} and P_{red} is strongly hindered by the formation of the polymeric gel-like film upon reduction. We tentatively ascribed P_{ox} and P_{red} to redox processes involving cobalt species and resulting in strong capacity fade. However, further investigation would be needed to clarify their exact origin.

The appearance and disappearance of P_{ox} and P_{red} clearly lead to capacity fading. However, significant fading was also observed in the case of electrode I at 2C and electrode O at C/5 and 2C, without any significant potential shift of P_{ox} and P_{red} (cf. Figs. 8a and b and 11b–d). In order to better understand this issue and since the increase in the cell resistivity has been assumed to be the main cause for the capacity fading [7,14] we decided to systematically evaluate the IR drop term by measuring the potential difference at the end of the discharge and the beginning of the charge. Fig. 12 shows the IR drop term upon cycling for the electrodes presented in Figs. 2, 5, 7 and 9. The first important information that can be extracted from these plots is that the formation of the SEI layer and the decomposition of the electrolyte do not lead to a significant increase of the cell resistivity, and the value of the IR drop term is generally stable, at least during the first few cycles (cf. Fig. 12). A significant decrease of the IR drop term is recorded even during the first ten cycles in the case of the long term cycling of electrodes I and O at C/5, C and 2C (cf. Fig. 12c and d). This is surprising since both the SEI layer and the gel-like film formation are usually considered to increase the cell resistivity. While the slow wetting of the electrode by the electrolyte could be responsible for this cell resistivity evolution upon cycling, it would be surprising that it constitutes the main reason since the decrease in cell resistivity is occurring during several days (even weeks). In any case, the measured IR drop term

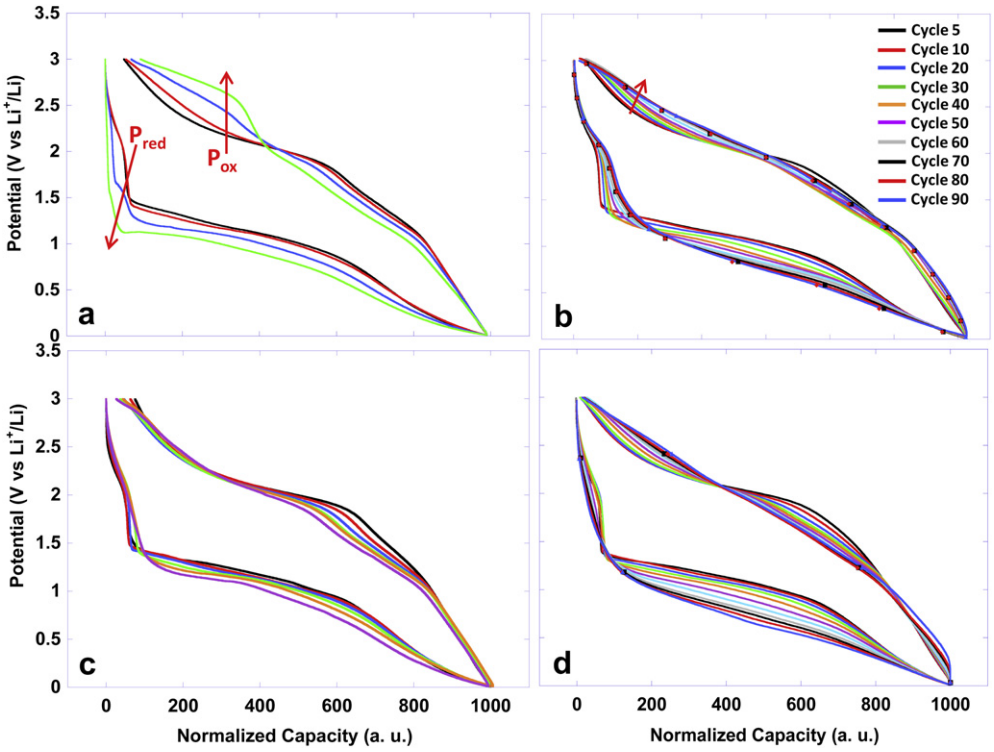

Fig. 11. Normalized voltage vs capacity profiles for electrodes I (a and b) and O (c and d), cycled at C rates of C/5 (a and c) and 2C (b and d).

being determined at the end of the discharge (reduction), the polymeric gel-like film is fully formed and is clearly not hindering the diffusion of Li^+ through the electrode nor the electron conductivity, at least not during the first few cycles.

From Fig. 12a, where the overpotential vs the number of cycles is plotted for electrodes pressed up to 10 t cm^{-2}. The unpressed electrode (0 t cm^{-2}, black squares in Fig. 12a) presents slightly higher overpotential, especially at a 2C rate. This is consistent with the fact that pressing electrodes reduces their porosity and thus improves their electrical connectivity [18]. However, even though similar overpotential values, during the first ten cycles, are recorded for both pressed and unpressed electrodes and for electrodes

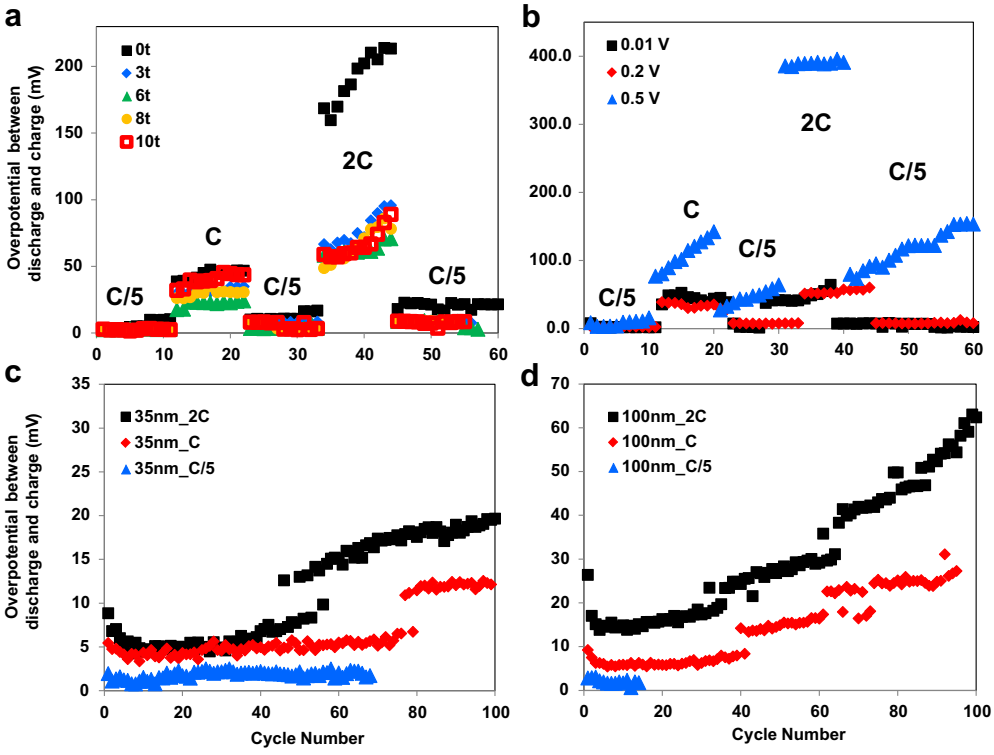

Fig. 12. Overpotential vs cycle number for the tests presented in a) Fig. 1a, b) Fig. 8a, c) Fig. 10a and d) Fig. 10b.

cycled with different lower cut-off voltages (cf. Fig. 12a and b), A dramatic difference in terms of capacity retention is observed (cf. Figs. 2a and 6a). Moreover, the capacity fade for 35 nm particles appeared to be larger than for 100 nm particles (cf. Fig. 8a and b), although the overpotential increase upon cycling in the latter case is much higher (cf. Fig. 12c and d). These results suggest the existence of an additional parameter responsible for the capacity fading upon cycling, which is not originating from the increase of the resistivity and/or possible dissolution of the active material.

EIS measurements were performed upon cycling in order to clarify this point, and the results are depicted in Fig. 13a as measurements 1–10 (thereafter called M1 to M10), corresponding to measurements before cycling (M1), after the first charge (M2), after the fifteenth charge (M3), etc. Two electrodes containing electrode O (cf. Table 1) were used as working electrodes and cycled at a 2C rate for 180 cycles. In order to better understand the influence of the polymeric gel-like film, its formation was favoured by holding the potential at ca. 0.01 V V vs Li^+/Li during 1 and 24 h after the first discharge. The plot of the capacity vs the number of cycles is shown in Fig. 13a for both electrodes and also for similar electrode cycled at 2C without any interruption during the cycling procedure (empty black squares) for sake of comparison. From

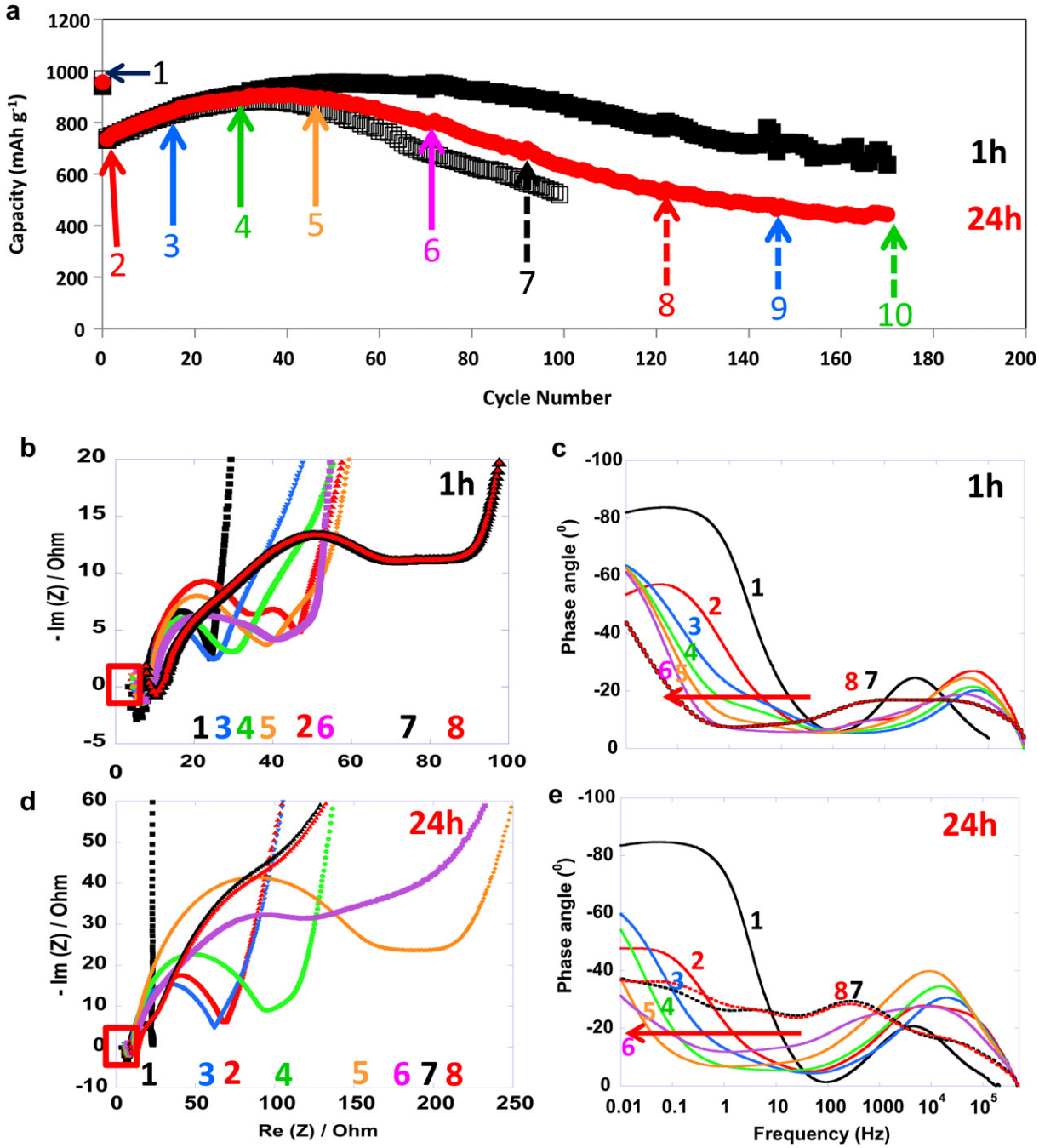

Fig. 13. a) Discharge capacity vs cycle number for electrodes O cycled at a 2C rate. Empty black squares correspond to an electrode cycled without interruption, black squares and red circles stand for electrodes held at 0.01 V vs Li^+/Li during 1 and 24 h after the first discharge, respectively. b) and d) Nyquist diagrams and c) and e) Bode diagrams recorded for electrodes held at 0.01 V vs Li^+/Li during 1 h (b and c) and 24 h (d and e). EIS measurements upon cycling obtained as indicated with arrows in a). (For interpretation of the references to colour in this figure legend, the reader is referred to the web version of this article.)

Fig. 13a we can say that excellent reproducibility is obtained up to the thirteenth cycle (M4), but thereafter, a significant improvement of the capacity retention is observed for the electrode after holding the potential at 0.01 V vs Li^+/Li during 1 h. Fig. 13b and d displays the Nyquist diagrams for the electrodes presented in Fig. 13a (M1 to M8). As described in Refs. [14,29] the Nyquist plot for composite electrodes of Co_3O_4 soaked with electrolyte can be separated in four different contributions that can be distinguished since their respective relaxation time constants are significantly different. Namely: i) contribution from the electronic conductivity of the electrode and ionic conductivity of the electrolyte solution (high frequencies, see the initial shift in resistivity in Fig. 13b and d identified by red squares), ii) contribution from the charge transfer processes (mid-frequency region, see the suppressed semi-circles in Fig. 13b and d), iii) contribution from the ionic conduction within a layer film (SEI and/or polymeric gel-like film) present at the surface of the active material particles (mid-frequency region, see the suppressed semi-circles in Fig. 13b and d) and iv) contribution from the bulk diffusional effects, mostly related to the diffusion of the salt within the electrolyte (low frequency region, see the Warburg diffusion tail in Fig. 13b and d).

Comparison of M1 in Fig. 13b and d (black squares) indicates that there is no significant difference between both electrodes in their initial state before cycling, neither in terms of low and mid-frequency region resistivity (respectively, ca. 8 and 16 Ω for both electrodes) nor in terms of Warburg diffusion tail. This proves that both electrodes are really alike as it was already pointed out when we discussed the cycling behaviour (Fig. 13a). However, after the first cycles differences start to appear between the electrodes held at 0.01 V vs Li^+/Li during 1 and 24 h. First of all, at the fifteenth cycle (M2) for the electrode held at 0.01 V vs Li^+/Li during 1 h, two depressed semi-circles can be observed, and are ascribable to the charge transfer resistance of the electrode and the presence of a layer film at the surface of the active material particles. This demonstrates that the polymeric gel-like film is still present at the end of the charge and that it is only partially removed upon oxidation. The fact that this second semi-circle is not visible in the case of the electrode held at 0.01 V vs Li^+/Li during 24 h is most probably due to the fact that the relaxation time constants for charge transfer resistance and ionic diffusion within the polymeric gel-like film cannot be discriminated. Indeed, the second semi-circle also disappeared after M2 for the electrode held at 0.01 V vs Li^+/Li during 1 h (cf. Fig. 13b). This suggests that the contribution of the polymeric gel-like film has grown enough for it cannot be distinguished from the charge transfer resistance contribution, although it can still be observed in M5, M6, M7 and M8. This contribution of the polymeric gel-like film results in deviation to the classic circular shape or the presence of quasi-horizontal plateau features. Similar features are observed for the electrode held at 0.01 V vs Li^+/Li during 24 h, confirming that the polymeric gel-like film is not completely removed upon oxidation, and thus might probably grow upon cycling. This is in agreement with what have been observed by transmission electron microscopy studies [13]. It is also worth mentioning that in both cases (i.e. potential held for 1 and 24 h), the mid-frequency region resistivity is first increased between M1 and M2 (cf. Fig. 13b and d) and then decreases between M2 and M3 (cf. Fig. 13b and d). Thereafter, it increases continuously upon cycling confirming what has been observed previously for the evolution of the overpotential values upon cycling (cf. Fig. 12d). The capacity fade occurs after the fiftieth cycle (M5 in Fig. 13a) for the electrode held at 0.01 V vs Li^+/Li during 24 h and after the seventieth cycle (M7 in Fig. 13a) for the electrode held at 0.01 V vs Li^+/Li during 1 h. From Fig. 13d we can say that capacity fading starts to occur, for the electrode held at 0.01 V vs Li^+/Li during 24 h, with a mid-frequency region resistivity of around ca. 200 Ω. In contrast, for the electrode held at 0.01 V vs Li^+/Li during 1 h, the capacity fade is observed with a mid-frequency region resistivity less than ca. 100 Ω, further confirming the fact that the increase in electrode resistivity is not the main factor inducing capacity fading.

Fig. 13c and e displays the Bode diagrams, where the phase angle is plotted vs the frequency of the perturbation. They are complementary representations of the Nyquist diagrams presented, respectively, in Fig. 13b and d and allow for a more straightforward observation of the relaxation time constant of the processes involved. Indeed, in this representation the processes related to the mid-frequency region appear at frequencies higher than 100 Hz, while processes related to the low frequency region (i.e. bulk diffusional effects, mostly diffusion of the salt within the electrolyte) appear at frequencies lower than 100 Hz. From the mid-frequency region we can confirm that the contribution of the diffusion within the polymeric gel-like film is better defined in the case of the electrode held at 0.01 V vs Li^+/Li during 1 h (appearance of a peak around 1000 Hz in M2). Indeed, the charge transfer resistance contribution appeared as a relatively narrow peak between 100 and 1000 kHz (cf. Fig. 13c), whereas, a broader peak is recorded in the case of the electrode held at 0.01 V vs Li^+/Li during 24 h. In the latter case the contribution of the diffusion within the polymeric gel-like film thus appears only as a broadening of the main peak around ca. 1000 Hz. More interestingly, the behaviour of both electrodes differs significantly in the low frequency region. Indeed, in both cases the curves appear to shift to lower frequencies upon cycling, suggesting that diffusion of the salt through the electrode is growingly hindered upon cycling. Moreover, this shift is significantly larger in the case of the electrode held at 0.01 V vs Li^+/Li during 24 h (cf. Fig. 13c and e), and eventually the curves disappear below the 0.01 Hz limit. Interestingly, the disappearance of the curves below the 0.01 Hz limit happens at the EIS M7 and M5, respectively, for the electrodes held at 0.01 V vs Li^+/Li during 1 and 24 h. As these EIS measurements correspond to the beginning of the capacity fade for these electrodes, it is straightforward to conclude that the capacity fade is related to the hindered diffusion pathway of the lithium through the electrode.

3.8. Model for the origin of the capacity fading in Co_3O_4 based composite electrodes

Based on the above observations we propose a new explanation for the capacity fade in conversion reaction materials, which differs from the commonly accepted hypothesis of the increase of the electrode resistivity upon cycling and is rooted on the incomplete removal of the polymeric gel-like film upon oxidation, resulting in the increase of the electrode tortuosity and thus lowering the lithium diffusivity through the electrode. Eventually, this leads to non-accessible regions of the electrode to the lithium ions, especially at high C rates when the time allowed for Li^+ diffusion is low. This model is in agreement with the results reported recently by Oumellal et al. [29], who demonstrated that the capacity fade for nanostructured silicon based electrodes is related to the formation of a thick solid electrolyte interface which limits the Li^+ diffusion through the electrode. This hypothesis allows for a better understanding of the experimental results. For instance, the fact that the capacity fade occurs more abruptly for 35 nm particles at high C rates as compared to larger particle sizes and/or at low C rates (cf. Fig. 8) is due to the catalytically enhanced electrolyte decomposition at the surface of the nano-sized particles [24]. Indeed, although the formation of the polymeric gel-like film would be enhanced at low C rates (longer polarization of the electrode at low potential), its formation will be favoured at the top surface of the electrode (directly in contact with the electrolyte) at high C rates (cf. Fig. 14, case b). In contrast, low C rates favour uniform growth of the

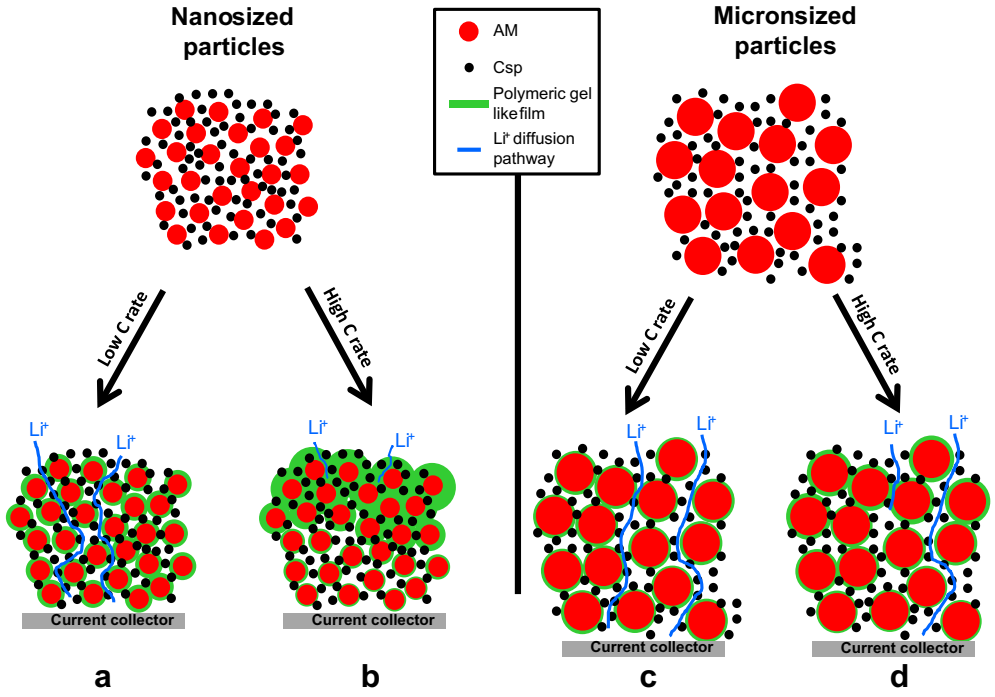

Fig. 14. Schematic representation of the growth of the polymeric gel-like film upon cycling for composite electrodes made with nano and micron size AM particles at low and high C rates.

polymeric gel-like film (cf. Fig. 14, case a), facilitating the Li^+ diffusion through the bulk of the electrode. This model is in agreement with the fact that when an electrode cycled at a 2C or C rate is experiencing a strong capacity fade, its full capacity can be recovered by lowering the C rate (cf. Fig. 8a), thus allowing the Li^+ to diffuse through the top polymeric gel-like film. In the case of larger particles, the electrolyte decomposition kinetics is much lower and thus the homogeneity of the polymeric gel-like film is greatly enhanced. This results in minimizing the limitation of the Li^+ diffusion (cf. Fig. 14, cases c and d), although it can be clearly evidenced by EIS measurements by favouring the growth of the polymeric gel-like film (i.e. holding the potential at 0.01 V vs Li^+/Li). The fact that capacity fade is significantly reduced when the electrode is left at OCV for several hours (24 h before each EIS measurements, cf. Fig. 13) supports the hypothesis that the capacity fade is rooted in the diffusion of Li^+ through the bulk of the electrode. In terms of practical applications, this would be an important factor to be taken into account as it would imply that batteries used in a discontinuous manner would cycled better than batteries used without interruption.

4. Conclusion

A systematic formulation study has been performed on Co_3O_4 based composite electrodes. Our results demonstrate that with electrodes made with Co_3O_4 particles smaller than 50 nm can be cycled with capacities of about ca. 1000 mAh g^{-1} for 100 cycles with optimized formulation which compares favourably with previous literature reports for no more than 10 stable cycles. Specific issues associated with materials reacting through conversion reactions (first cycle coulombic inefficiency, voltage hysteresis and capacity fade) have been discussed at the light of these results. It appears that under optimized formulation conditions the first cycle coulombic efficiency can be increased. Voltage hysteresis was systematically measured and no significant differences were recorded. Furthermore, the values of the IR drop terms and were found to be negligible as compared to those of the voltage hysteresis, suggesting that the latter are rooted in thermodynamic reasons associated with the conversion reaction mechanism itself. Systematic record of the IR drop term upon cycling and EIS measurements allowed us to propose a mechanism to account for capacity fade in conversion reaction materials. Contrary to previous assumptions dealing with enhanced electrode resistivity, a model is proposed based on the inhomogeneous growth of the polymeric gel-like film (formed upon reduction and incompletely removed upon oxidation) within the bulk of the electrode having a negative effect on lithium diffusion, which allows for a much more consistent explanation of the capacity decay observed experimentally.

Acknowledgement

This work was made with the support of Ficosa and Premo through the Battman Consortium (Acc1ó (Generalitat de Catalunya), Feder). We acknowledge Ministerio de Ciencia e Innovación for grant MAT2011-24757 and are grateful to Bernard Lestriez (IMN, Nantes, ALISTORE ERI formulation summer school), Dominique Larcher for helpful discussions, Gerard Tobias for providing the purified carbon nanotubes used in this study, Julio Fraile for BET measurements and Deyana Tchitchekova for help with numerical calculations allowing for a systematic measurement of the overpotential values.

References

[1] M.R. Palacín, Chem. Soc. Rev. 38 (2009) 2565.
[2] C.M. Park, J.H. Kim, H. Kim, H.J. Sohn, Chem. Soc. Rev. 39 (2010) 3115.
[3] J. Cabana, L. Monconduit, D. Larcher, M.R. Palacín, Adv. Mater. 22 (2010) E170.
[4] B. Lestriez, S. Desaever, J. Danet, P. Moreau, D. Plée, D. Guyomard, Electrochem. Solid-State Lett. 12 (2009) A76.
[5] B. Lestriez, C. R. Chimie 13 (2010) 1341.
[6] J. Li, H.M. Dahn, L.J. Krause, D.-B. Le, J.R. Dahn, J. Electrochem. Soc. 155 (2008) A812.
[7] D. Larcher, G. Sudant, J.-B. Leriche, Y. Chabre, J.-M. Tarascon, J. Electrochem. Soc. 149 (2002) A234.

[8] G. Binotto, D. Larcher, A.S. Prakash, R. Herrera Urbina, M.S. Hegde, J.-M. Tarascon, Chem. Mater. 19 (2007) 3032.
[9] K.M. Shaju, F. Jiao, A. Débart, Peter G. Bruce, Phys. Chem. Chem. Phys. 9 (2007) 1837.
[10] S. Grugeon, S. Laruelle, R. Herrera-Urbina, L. Dupont, P. Poizot, J.-M. Tarascon, J. Electrochem. Soc. 148 (2001) A285.
[11] P. Poizot, S. Laruelle, S. Grugeon, L. Dupont, J.-M. Tarascon, Nature 407 (2000) 496.
[12] D. Barreca, M. Cruz-Yusta, A. Gasparotto, C. Maccato, J. Morales, A. Pozza, C. Sada, L. Sánchez, E. Tondello, J. Phys. Chem. C 114 (2010) 10054.
[13] S. Laruelle, S. Grugeon, P. Poizot, M. Dollé, L. Dupont, J.-M. Tarascon, J. Electrochem. Soc. 149 (2002) A627.
[14] J.-G. Kang, Y.-D. Ko, J.-G. Park, D.-W. Kim, Nanoscale Res. Lett. 3 (2008) 390.
[15] M. Dollé, P. Poizot, L. Dupont, J.-M. Tarascon, Electrochem. Solid-State Lett. 5 (2002) A18.
[16] A. Ponrouch, M.R. Palacín, J. Power Sources 196 (2011) 9682.
[17] B. Ballesteros, G. Tobias, L. Shao, E. Pellicer, J. Nogués, E. Mendoza, M.L.H. Green, Small 4 (2008) 1501.
[18] C. Fongy, A.-C. Gaillot, S. Jouanneau, D. Guyomard, B. Lestriez, J. Electrochem. Soc. 157 (2010) A885.
[19] X. Xiang, Z. Huang, E. Liu, H. Shen, Y. Tian, H. Xie, Y. Wu, Z. Wu, Electrochim. Acta 56 (2011) 9350.
[20] A. Ponrouch, P.L. Taberna, P. Simon, M.R. Palacín, Electrochim. Acta 61 (2012) 13.
[21] P.L. Taberna, S. Mitra, P. Poizot, P. Simon, J.-M. Tarascon, Nat. Mater. 5 (2006) 567.
[22] X.W. Lou, D. Deng, J.Y. Lee, J. Feng, L.A. Archer, Adv. Mater. 20 (2008) 258.
[23] E. Peled, J. Electrochem. Soc. 126 (1979) 2047.
[24] S. Grugeon, S. Laruelle, L. Dupont, J.-M. Tarascon, Solid State Sci. 5 (2003) 895.
[25] R. Fong, U.Y. Sacken, J.R. Dahn, J. Electrochem. Soc. 137 (1990) 2009.
[26] P.A. Connor, J.T.S. Irvine, Electrochim. Acta 47 (2002) 2885.
[27] P. Balaya, A.J. Bhattacharyya, J. Jamnik, Y.F. Zhukovskii, E.A. Kotomin, J. Maier, J. Power Sources 159 (2006) 171.
[28] A.-L. Dalverny, J.-S. Filhol, M.-L. Doublet, J. Mater. Chem. 21 (2011) 10134.
[29] Y. Oumellal, N. Delpuech, D. Mazouzi, N. Dupré, J. Gaubicher, P. Moreau, P. Soudan, B. Lestriez, D. Guyomard, J. Mater. Chem. 21 (2011) 6201.